Photoacoustic Tomography Shows the Branching Pattern of Anterolateral Thigh Perforators In Vivo

Abstract

Background

The distal branching pattern of perforators is associated with thin anterolateral thigh (ALT) flap failure. The purpose of this study is to investigate the feasibility of using photoacoustic tomography (PAT) as a diagnostic imaging modality to identify ALT perforators and their branching patterns in the subcutaneous layer.

Methods

Ten thighs in five healthy males were studied. The anterolateral aspect of the mid-thigh was examined using PAT. The correlation between PAT and ultrasound (US) findings was evaluated. To determine the detectability of PAT by depth, the depth of vessels in the stem portion was compared to the depth of the deep fascia measured by US. Branching patterns of vessels in the adipose and suprafascial layers were evaluated by three-dimensional observation.

Results

A total of 18 perforators were visualized by PAT. PAT and US had comparable diagnostic potential for the detection of perforators. PAT visualized microvessels in the subcutaneous layer, especially those in oblique or horizontal orientations. The estimated mean depth of visualized vessels was 9 mm; the maximum was 13 mm. There was a strong correlation between the depth of visualized vessels in the stem portion and the depth of the deep fascia. Three-dimensional observation of PAT images showed the branching morphology of perforators.

Conclusions

This study showed the applicability of PAT to identification of the branching patterns of ALT perforators in vivo although limited visualization of subfascial vessels is a technical issue. We believe PAT has the potential to be a new imaging modality for thin ALT flap surgery.

Key words

Anterolateral thigh, imaging, perforator, photoacoustic tomography, thin flap

Introduction

Flap thinning[1] is technically challenging. In particular, a high rate of failure has been reported for the thin anterolateral thigh (ALT) flap.[2] Previous experimental studies have suggested that skin perfusion is changed during thinning as a result of injuries to vessels in the suprafascial layer.[3] Thus, an appreciation of the individualized vascular anatomy of the thigh is essential for thin flap planning; however, suitable imaging methods that can be used safely and easily *in vivo* are lacking. Photoacoustic tomography (PAT) is an emerging vascular imaging modality that has been used in basic research and clinical practice, which allows for visualization of subcutaneous vessels on the basis of the photoacoustic mechanism. Energy from a near-infrared pulse laser is introduced into hemoglobin. As a result, red blood cells become swollen and release ultrasonic waves, which allows vessels to be visualized without contrast agents.[4] The purpose of this study is to investigate the feasibility of using PAT as an imaging tool for identifying branching vessels in the subcutaneous layer associated with the thin ALT flap.

Materials and methods

After approval by our institutional ethics committee and clinical trial registration, we recruited five healthy male adults (mean age, 41 years; mean body mass index, 23.1 kg/m^2) for this study. PAT was performed bilaterally in all subjects.

The PAT we employed was the same system that was used for a previous study on breast cancer angiogenesis. In that study, the estimated maximum depth of vessels visualized was 27 mm.[5] The system comprised a Ti:sapphire laser transmitter and a tabletop scanning platform (Supplemental Digital Content Figure 1). The wavelength of the laser was 797 nm. The maximum laser power was set to less than the half the maximum permissible exposure recommended by the American National Standards Institute. Multiple ultrasonic transducers were placed into a hemispherical cup built into the platform. Each subject was placed on the platform in the semi-prone position with the anterolateral surface of the mid-thigh facing the cup. The space between the skin and the cup was filled with de-aired water for smooth transmission of ultrasonic waves. Each scan took approximately 2 minutes for a 14 × 14 cm^2 region. Acquired data were processed three-dimensionally using laboratory-made imaging software. Visualization of vessels in the adipose or suprafascial layer was performed using the following steps. First, the surface of the skin was identified automatically using signals from the dermis. Next, color gradation was applied to the images according to the depth from the skin surface. Subdermal venous networks in the most superficial layer were visualized in blue. Finally, vessels in the adipose layer or deeper were visualized independent of the venous networks by semi-automatically cropping out the superficial layer that included the networks (Fig. 1).

To study the diagnostic potential of PAT, the correlation between the locations of perforators identified on PAT versus conventional ultrasound (US) was evaluated. To determine the detectability of PAT by depth, the depth of vessels in the stem portion was measured and compared to the depth of the deep fascia measured using US. The orientation of perforators in the stem portion was also evaluated. The branching morphology of vessels in the adipose and suprafascial layers was evaluated using three-dimensional observation.

Results

PAT visualized the branching vessels of perforators in the subcutaneous layer in all subjects. PAT showed 18 perforators and US showed 15 perforators, all of which were visualized by PAT. However, discrepancies in location of less than 10 mm were frequently observed. The estimated mean depth of vessels visualized by PAT was 9 mm; the maximum was 13 mm. Unlike US, PAT does not visualize the soft tissue components. Comparison of the depth of a vessel visualized by PAT with the depth of the deep fascia visualized by US at the corresponding site revealed a strong correlation (Pearson’s correlation = 0.8). Among the 18 perforators, nine had an orientation of approximately 30 degrees relative to the horizontal plane and the remaining nine had an orientation of 30–60 degrees.

Three-dimensional observation of PAT images showed the branching pattern of perforators. Fourteen Type I and four Type II perforators according to a classification system proposed by Schaverien et al.[6] were observed. Figure 2 is a representative image showing a Type II perforator with horizontal branches visualized in the deepest layer and oblique branches more superficially (see also Supplemental Digital Content Video 1). Such branching vessels in the suprafascial layer were almost always undetectable by Doppler mode of US (Supplemental Digital Content Figure 2).

Discussion

This is the first report to show the feasibility of using PAT imaging to visualize the branching morphology of perforators in the subcutaneous layer in the anterolateral thigh. The three-dimensional nature of PAT imaging contributed to identification of the branching morphology of perforators.

Compared with conventional US, PAT visualized vessels to the level of the deep fascia. By contrast, vessels deeper than the fascia were undetectable, suggesting that the deep fascia could be a factor limiting the depth performance of PAT. The lack of anatomical references of PAT imaging is a barrier to its intraoperative use. Cooperation of US with PAT would resolve these issues.

PAT has two other technical limitations. First, there are currently no established methods to distinguish arteries from veins using PAT, thus a triple bundle appearance was common, especially in vessels near the stem portion (Fig. 2). The subdermal venous networks were distinguishable owing to their superficial location and polygonal morphology.[7] Second, the orientation of a vessel affects its visualization by PAT. This is known as the limited view problem.[8] More vertically distributed vessels are reportedly less likely to be visualized. Indeed, no vertical vessels were observed in this study, although vessels at an angle of approximately 60 degrees were visualized. This might be the reason why no Type III perforators were found in this study.

Although further technical refinements are needed for PAT to establish its clinical utility, we believe that PAT would be a promising new imaging modality for thin ALT flap surgery.

Authors' role/participation in the authorship of the manuscript

SS conducted the study and IT performed the experiments. HS developed imaging software. IT, AY and SS analyzed the data. All the authors contributed to writing of the manuscript.

Acknowledgement

This work was funded by the ImPACT Program of the Council for Science, Technology and Innovation (Cabinet Office, Government of Japan). Canon invented the photoacoustic imaging system used in this study. We would like to express our sincere gratitude to all our collaborators: Tomoko Kosaka, Kazuko Kobayashi, Yasufumi Asao, Shuichi Kobayashi and Takayuki Yagi.

References

1) Kimura N, Satoh K. Consideration of a thin flap as an entity and clinical applications of the thin anterolateral thigh flap. Plast Reconstr Surg. 1996; 97: 985-992.

2) Ross GL, Dunn R, Kirkpatrick J, Koshy CE, Alkureishi LW, Bennett N, Soutar DS, Camilleri IG. To thin or not to thin: the use of the anterolateral thigh flap in the reconstruction of intraoral defects. Br J Plast Surg. 2003; 56: 409-413.

3) Alkureishi LWT, Shaw-Dunn J, Ross GL. Effects of thinning the anterolateral thigh flap on the blood supply to the skin. Br J Plast Surg. 2003; 56: 401-408.

4) Wang LV, Hu S. Photoacoustic tomography: in vivo imaging from organelles to organs. Science. 2012; 335(6075):1458-1462.

5) Toi M, Asao Y, Matsumoto Y, Sekiguchi H, Yoshikawa A, Takada M, Kataoka M, Endo T, Kawaguchi-Sakita N, Kawashima M, Fakhrejahani E, Kanao S, Yamaga I, Nakayama Y, Tokiwa M, Torii M, Yagi T, Sakurai T, Togashi K, Shiina T. Visualization of tumor-related blood vessels in human breast by photoacoustic imaging system with a hemispherical detector array. Sci Rep. 2017; 7: doi10.1038/srep41970

6) Schaverien M, Saint-Cyr M, Arbique G, Hatef D, Brown SA, Rohrich RJ. Three- and four-dimensional computed tomographic angiography and venography of the anterolateral thigh perforator flap. Plast Reconstr Surg. 2008; 121: 1685-1696.

7) Imanishi N, Kishi K, Chang H, Nakajima H, Aiso S. Three-dimensional venous anatomy of the dermis observed using stereography. J Anat. 2008; 212: 669-673.

8) Xu Y, Wang LV. Reconstructions in limited-view thermoacoustic tomography. Am Assoc Phys Med. 2004; 31: 724-733.

Figure legends

Fig. 1

Anteroposterior photoacoustic tomography images in the all-layer (left) and deep-layer views (right). The color corresponds to the depth from the skin surface. Note that the blue superficial venous networks in the all-layer image are not shown in the deep-layer image; deep branching vessels in red are visualized separately. Scale bar = 20 mm.

Fig. 2.

Photoacoustic tomography projection images showing a Type II branching pattern in a perforator. Insets are lateral views for the regions indicated in the anteroposterior image. In the inset A–B, a perforator bifurcates into vessels coursing horizontally and oblique to the skin surface. In the inset C–D, a branch coursing obliquely from the bifurcation changes its direction, becoming more horizontal in the distal portion. Note the triple bundle appearance of the branches (arrowhead). Scale bars = 10 mm. See also Supplementary video 1.

Supplemental Digital Content Figure 1

Schematic of the photoacoustic tomography system.

Supplemental Digital Content figure 2

Images show a difference in visual performance between PAT and Doppler ultrasound. Note that the oblique portion of the perforator system in the subcutaneous layer shown by PAT is not visualized by Doppler US (arrowhead).

Supplemental Digital Content Video 1

The video highlights three-dimensional visualization of the branching vessels in Fig. 2. The color of the vessels corresponds to the depth from the skin. X, Y, and Z coordinates indicate the medial, distal, and posterior directions, respectively.

Figure 1

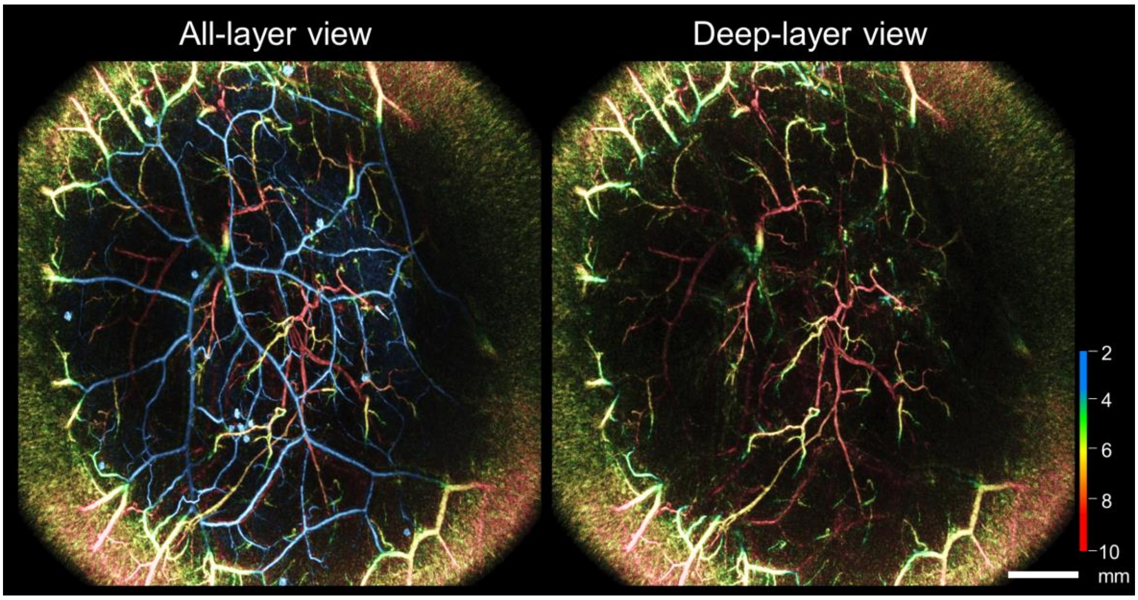

Figure 2

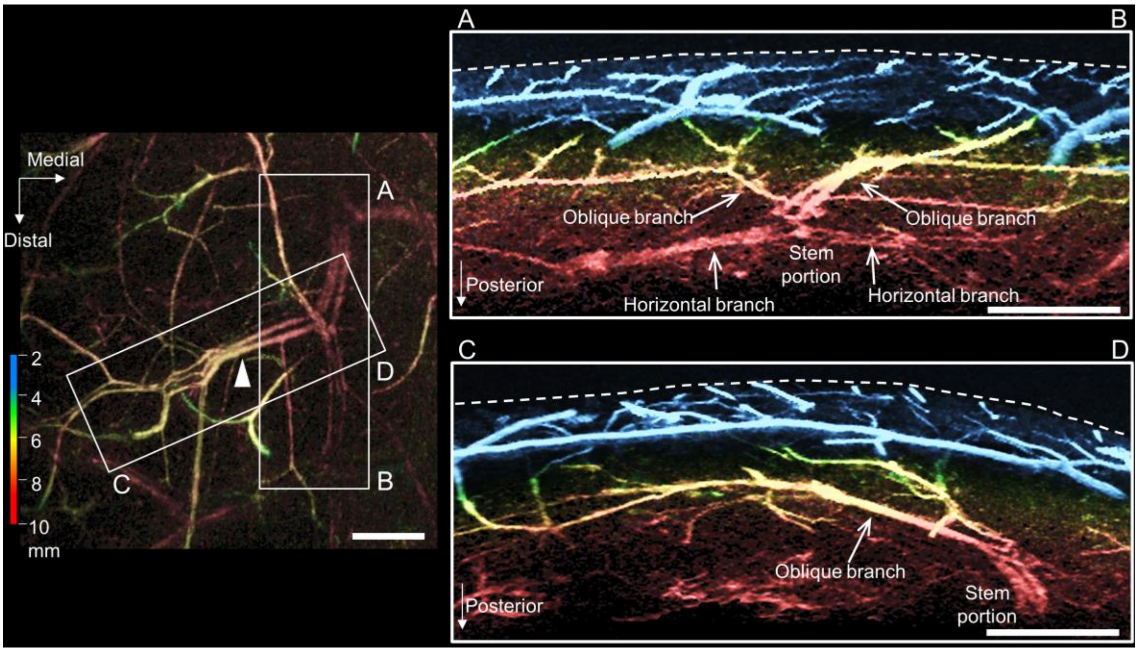

Supplemental Digital Content Figure 1

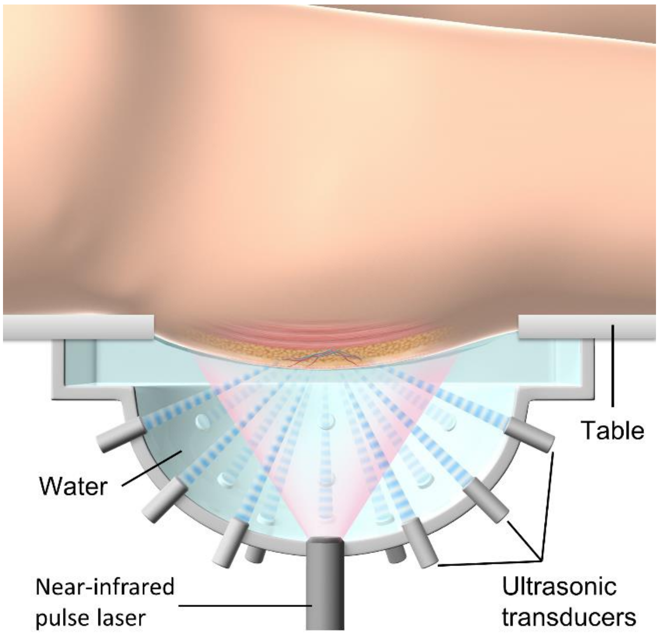

Supplemental Digital Content Figure 2

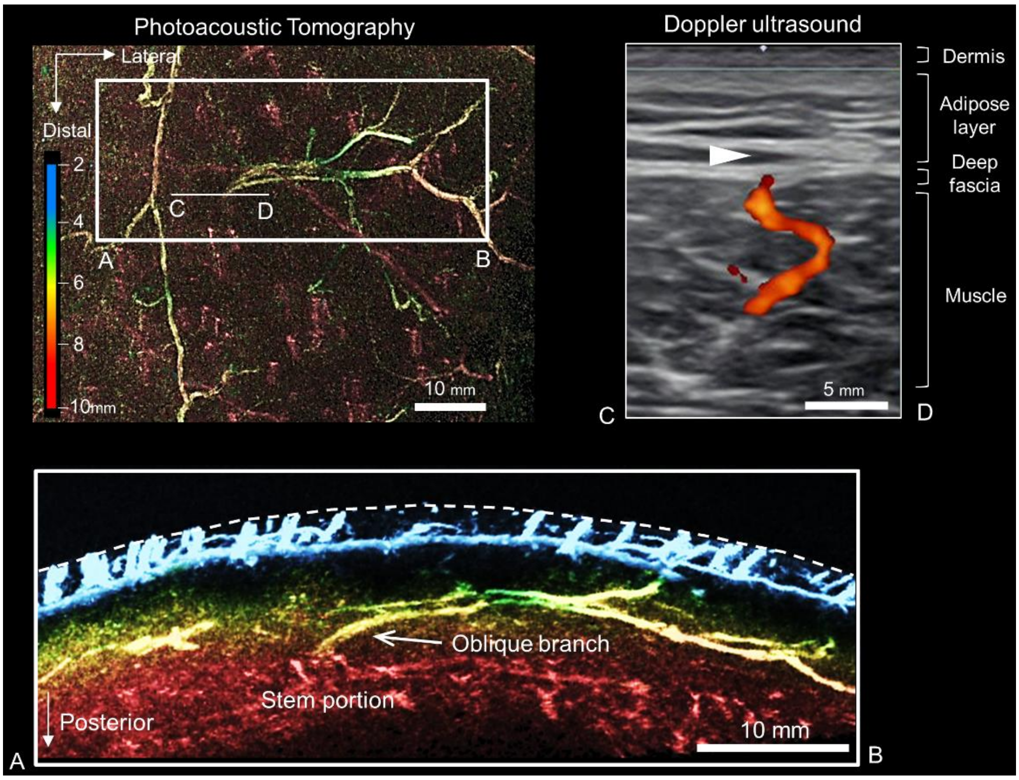

Supplemental Digital Content Video 1

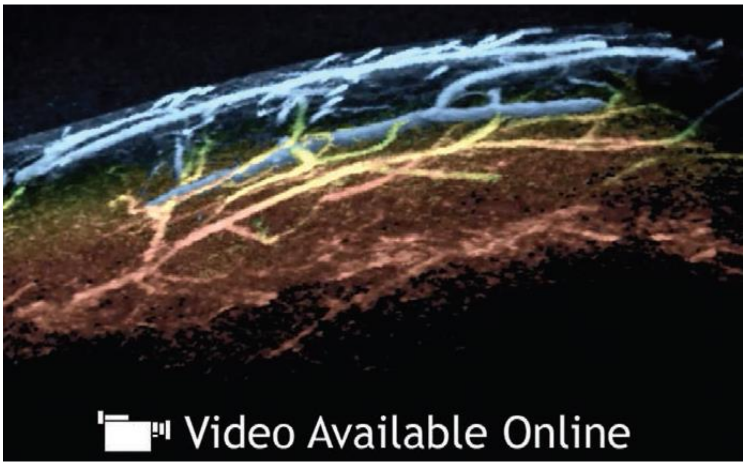

http://links.lww.com/PRS/C748

Preoperative vascular mapping for anterolateral thigh flap surgeries: A clinical trial of photoacoustic tomography imaging

Itaru Tsuge, MD 1

Susumu Saito, MD, PhD 1

Goshiro Yamamoto, PhD 2

Hiroyuki Sekiguchi, PhD 3

Aya Yoshikawa 4

Yoshiaki Matsumoto, MD, PhD 4

Shigehiko Suzuki, MD, PhD 1, 5

Masakazu Toi, MD, PhD 4

1. Department of Plastic and Reconstructive Surgery, Graduate School of Medicine, Kyoto University, Kyoto, Japan

2. Department of Medical Informatics, Graduate School of Medicine, Kyoto University, Kyoto, Japan.

3. Department of Diagnostic Imaging and Nuclear Medicine, Graduate School of

Medicine, Kyoto University, Kyoto, Japan.

4. Department of Breast Surgery, Graduate School of Medicine, Kyoto University, Kyoto, Japan.

5. Department of Plastic and Reconstructive Surgery, Hamamatsu Rosai Hospital, Shizuoka, Japan

Corresponding to:

Itaru Tsuge, M.D.

Department of Plastic and Reconstructive Surgery, Graduate School of Medicine, Kyoto University, 54 Shogoin Kawahara-cho, Sakyou-ku, Kyoto 606-8507, Japan

Fax: +81-75-751-4340, Tel: +81-75-751-3613

E-mail: itsuge@kuhp.kyoto-u.ac.jp

Disclosure:

The authors have no financial interest to declare in relation to the content of this article.

This clinical trial was registered as UMIN000028001.

Acknowledgements:

This work was funded by the ImPACT Program of the Council for Science, Technology and Innovation (Cabinet Office, Government of Japan). We would like to express our sincere gratitude to all of our collaborators: Tomoko Kosaka, Kazuko Kobayashi, Ishii Tomoko, Minako Chaya, Takeshi Namita, Ryoma Bise, Norihiko Utsunomiya, Yasufumi Asao, Keishi Saito, Shuichi Kobayashi, Tsuyoshi Shiina and Takayuki Yagi.

Running title:

Vascular mapping using PAT

Abstract

Background: Photoacoustic tomography (PAT) is a non-invasive vascular imaging modality that uses near-infrared pulse laser beams and ultrasound (US) to visualize vessels. We previously demonstrated the utility of PAT for visualizing anterolateral thigh (ALT) perforators in a clinical study of 10 thighs in 5 healthy adults. Evaluation of the correlation between PAT and US findings showed that PAT had comparable diagnostic potential but was superior in visualizing subcutaneous microvessels; however, there was no comparison with intraoperative findings. In this study, we used a newly developed technique to transfer a PAT image to a body-attachable transparent sheet to compare PAT and intraoperative findings.

Methods: Eight patients were recruited in this prospective study. Patient age ranged from 32 to 79 years (average 60). Seven ALT flaps were applied in head and neck reconstruction. One flap was elevated in chest wall reconstruction. Each PAT scan of an 18 × 13.5-cm region took approximately 5 minutes. Acquired data were processed 3-dimensionally using a novel imaging software program. Perforator vessel data from PAT imaging were traced and corrected for projection onto medical film sheets. The correlation between the perforator stem portions predicted by PAT and the intraoperative findings at the level of the fascia-penetrating points was evaluated, and distal branching patterns were analyzed.

Results: PAT imaging showed 16 perforators in 8 thighs. Intraoperative surgical findings revealed that all the perforator penetrating points at the deep fascia level matched the PAT findings within 10 mm. None of the 8 ALT flaps demonstrated postoperative complications. The perforator complexes were classified as type I in 3 cases (19%), type II in 8 cases (50%), and type III in 5 cases (31%).

Conclusions: PAT imaging matched the intraoperative findings within 10 mm. Preoperative vascular evaluation allows for the creation of a vascular map for facilitating ALT flap surgeries.

Introduction

The anterolateral thigh (ALT) flap has the advantages of minimal donor-site morbidity, a long vascular pedicle, and the fact that it is created during the same surgery as that performed for tumor resection [1)]. Anatomic studies using computed tomography (CT) angiography revealed variations in the distal branching pattern of perforators in the adipose layer [2)]. Preserving obliquely and horizontally coursing branches in the adipose layer is important, especially in cases where the flap is thinned [3)].

Photoacoustic tomography (PAT) is an emerging vascular imaging modality that uses near-infrared pulse laser beams and ultrasound (US) to visualize vessels [4)]. Energy from a near-infrared pulse laser is absorbed into hemoglobin; this causes red blood cells to become swollen and emit ultrasonic waves, which allows vessels to be visualized without contrast agents. We previously used this technology to evaluate distal ALT perforator vessels in the subcutaneous layer. In 2018, we showed the feasibility of using PAT as a diagnostic imaging modality to identify ALT perforators and their distal branching patterns in the subcutaneous layer by studying 10 thighs in 5 healthy adults [5)].

Evaluation of the correlation between PAT and US findings indicated that the 2 methods had comparable diagnostic potential for the detection of perforators at the level of the deep fascia; however, PAT was superior in visualizing subcutaneous microvessels with high resolution, especially those in oblique or horizontal orientations.

However, an unsolved problem remained, namely the lack of a surgical navigation method to directly apply the detailed and high-resolution vascular images. We developed a technique to transfer 3-dimensional coordinate data of perforators obtained by PAT imaging to a body-attachable transparent sheet. The present study aimed to apply this non-invasive *in vivo* imaging method to patients undergoing ALT flap surgery. Its goals were 2-fold: first, to establish a mapping surgery method using PAT to create vascular mapping sheets able to be attached to the body surface; second, to clarify the accuracy of PAT mapping results by comparing them with surgical findings.

Patients and Methods

This study was approved by the ethics committee of the Kyoto University Graduate School of Medicine (C1298) and was conducted in accordance with the Declaration of Helsinki. Written informed consent was obtained from all patients. The inclusion criteria were as follows: clinical patients who were ≥20 years old at the time of diagnosis and who were scheduled to receive reconstructive surgery using a free ALT flap. The exclusion criteria were as follows: any wounds or pain in the lower legs, difficulty maintaining a semi-prone position, pregnancy or suspicion of pregnancy, ongoing photodynamic therapy with photosensitizing agents such as Photofrin, implantation with a cardiac pacemaker, and any other condition considered to render a patient unsuitable for the study. Eight patients (3 women and 5 men) were recruited from among 20 who met the inclusion criteria. The reasons for patient exclusion were as follows: 5 lived far away, 3 were undergoing emergent or semi-emergent surgery, 2 had pain in their knees, and 2 had difficulty maintaining a semi-prone position. The age of the patients ranged from 32 to 79 years (average 60), and the body mass index ranged from 17.6 to 30.1 kg/m^2

(average 23.1). The bilateral thighs in the 8 patients were examined by PAT. The laterality of the thigh undergoing surgery was determined based on patient request and which thigh was undergoing simultaneous surgery for tumor resection.

Schedule from PAT imaging to surgery

The experimental steps are shown in **Table 1**. PAT imaging was scheduled 7 to 10 days before the day of surgery. Day 1: The bilateral anterolateral aspects of the mid-thigh were examined by US and PAT. Day 2: Perforator vessel data from PAT imaging were traced and corrected for projection mapping. Day 3: Vascular coordinate data were projected onto transparent medical film sheets and drawn manually with three color codes. Day 4: The sheets were sterilized for surgery. On the day of surgery, the sheets were attached to the patient's thighs.

PAT imaging system

The PAT imaging system (PAI-05) was equipped with a hemispherical detector array

(HDA) that received the PA signal, and was developed in cooperation with Canon, Inc., Hitachi, Ltd., and Japan Probe Co., Ltd [6]. The basic mechanism of this imaging system was explained in our previous papers [7, 8, 9]. In brief, the system had an HDA with a near-infrared irradiation mechanism embedded in its center. The HDA was filled with de-aired water for the smooth transmission of ultrasonic waves. When the pulsed laser light illuminated blood vessels, ultrasonic waves were emitted and detected by multiple transducers in the HDA. The laser in this device was a Ti:sapphire laser, which had a wavelength of 797 or 850 nm. The power level of the laser was restricted to the maximum permissible exposure limit recommended by the American National Standards Institute as unlikely to cause injury [10].

Visualization and 3-dimensional analyses

First, a color Doppler US test was performed using a HI VISION Ascendus ultrasound machine (Hitachi, Tokyo, Japan) in the PAT imaging room. The US-predicted perforator penetrating points of the fascia lata were marked in red ink. Multiple dots spaced at 4-cm intervals were marked on the anterolateral aspect with purple ink, which was detectable by PAT (**Figure 1A**). Next, each patient was laid on the platform in the semi-prone position with the anterolateral aspect of the thigh facing the HDA (**Figure 1B**). Each scan of an 18 × 13.5-cm region took approximately 5 minutes. The red and purple ink marked on the thigh were preserved by covering the skin with transparent medical film sheets until the day of surgery. Acquired data were processed 3-dimensionally using a newly developed imaging software program (Kurumi; Kyoto University, Kyoto, Japan). The surface of the skin was identified automatically using signals from the dermis (the cloth simulation method, in which the object is calculated from the identified dermal signal to define the cutaneous surface, as if the object was covered by a thin cloth) [11]. Color gradation was applied to the images according to the depth from the skin surface (**Figure 2A**). Finally, morphologically identified subdermal venous networks in the superficial layer [12] were removed to permit semi-automatic visualization of the subcutaneous vessels in the deeper layer using a deep-layer view.

The perforator analysis

The PAT-predicted perforator stem portion was defined as the deepest point at which PAT imaging visualized vessels in a triple-bundled appearance (**Figure 2B**). In surgery, perforator vessels were detected beneath the deep fascia. Fascia-penetrating points were defined as points at which bundled vessels including a pulsating artery entered the deep fascia. The accuracy of PAT mapping was assessed based on the differences between the PAT-predicted perforator stem portion and intraoperative identification of the fascia penetrating point.

Perforator types in the subcutaneous layer were identified according to the perforator complex patterns defined by Shaverien et al. [2)]. This classification is based on the presence of oblique or descending branches coursing through the adipose layer, and on the identification of horizontal branches at the suprafascial level. Examples of an oblique branch and a horizontal branch in PAT imaging are shown in **Figure 2C**. The type I perforator complex has oblique branches without any horizontal branches, the type II perforator complex has oblique branches and horizontal branches, and the type III perforator complex has descending branches and horizontal branches.

Projection mapping

First, the courses of perforators and the linking vessel networks on each PAT image were traced using the Kurumi software program (**Figure 2D**). Next, a correction processing software program developed by G.Y. on Xcode with Objective-C, OpenCV, and OpenGL was applied to show the blood vessels present beneath the sheet when an operator viewed the sheet from a position perpendicular to the skin surface (**Figure 3A**). In the program, two geometrical conversions were considered: vessel to skin and skin to film. The horizontal plane of each skin surface point was calculated, after which each perpendicular line from the detected horizontal plane was defined. The coordinate of the point at which the perpendicular line crossed the subcutaneous vessel was then converted to a skin surface coordinate. Finally, the curved skin surface information was translated into a flat plane for projection mapping onto a film sheet.

Preparation of mapping sheets

A Tegaderm® 10 × 12 cm (3M, MN, USA) medical transparent sheet was applied as a vascular mapping sheet. The image projected onto the film sheet was manually drawn in ink (**Figure 3B**). The color codes for the vascular films were as follows: black, indicating >9-mm deep; blue, indicating 7- to 9-mm deep; and red, indicating <7-mm deep. The vascular mapping sheets were sterilized using STERRAD® (Johnson & Johnson, NJ, USA) (**Figure 3C**). We opened the sterilized sheets in a clean field and attached them along the purple grid points (each 4 cm apart) on the patient's thigh. Two mapping sheets were attached, overlapping the central scanning point. The skin was incised through the transparent mapping sheets.

Results

Preoperative US showed 16 perforators in 8 thighs. The average depth from skin to fascia was 11 cm. PAT imaging also showed 16 perforators in 8 thighs; however, there were discrepancies in the predictions in 2 individuals (cases 2 and 7 in **Table 2**). Comparison between the PAT-predicted perforator stem portion and intraoperative findings of the fascia-penetrating points showed a complete match in 16 perforators (**Table 2**). Skin incision and intraoperative tissue traction interfered with precise measurement; however, the location differences between PAT-predicted points and intraoperative fascia-penetrating points were estimated to be within 10 mm for all perforators. Three-dimensional observation of PAT images showed the perforator branching patterns. The types of perforator complexes were as follows: 3 type I (19%), 8 type II (50%), and 5 type III (31%). None of the 8 ALT flaps demonstrated any postoperative complications. Thinning procedures were performed in 2 cases that required thin flaps for the reconstruction of the oral cavity and pharynx (**Figure 4 and Supplemental figure 1**).

Discussion

Navigation systems using 3-dimensional information obtained by preoperative imaging have been adopted to make surgeries safer and more reliable. In reconstructive flap surgery, however, there has been no technique for performing flap elevation using precise vascular information. This study demonstrates the accuracy of the vessel map generated by PAT, and for the first time shows that PAT can be used as a tool to directly support flap surgery. This is also the first study to demonstrate a body-attachable vascular map based on PAT imaging. We showed the accuracy of the positions of PAT-predicted perforator stem complexes by comparing them with intraoperative findings.

PAT was developed to visualize blood vessels noninvasively. The quality of 3-dimensional visualization has rapidly progressed. Our team previously reported the visualization of tumor-related blood vessels in breast cancer at depths of up to 27 mm [9]. In 2018, we reported the feasibility of using PAT imaging in ALT flap perforator analysis in the examination of healthy subjects [5]. We evaluated 10 thighs in 5 healthy adults by PAT and US. All 15 perforators detected by US were visualized by PAT, with location discrepancies of less than 10 mm. Furthermore, PAT was previously shown to be superior to US for visualizing subcutaneous vessels. However, that study did not examine intraoperative surgical findings [5]. In the present clinical trial, we confirmed the safety of PAT imaging in clinical patients and the accuracy of the PAT-predicted perforator stem portion in comparison with the actual perforator positions at the level of the deep fascia.

All of the previously published papers concerning "perforator mapping" have indicated the locations of perforator points arising from the deep fascia [13, 14], but none have included information on the detailed courses of perforators in the subcutaneous layer. Our study is therefore the first to demonstrate perforator mapping of the subcutaneous perforator networks *in vivo* and to prepare an intraoperatively useful mapping sheet that can be attached to the body surface. Our method of establishing reference points on the body surface is important for applying imaging data to an actual patient's body in the future. Shen et al. used plastic tubes as reference points for CT angiographic perforator mapping; however, they used only 2 points at the center of the thigh [15]. The laser wavelengths used in PAT imaging make it possible to visualize body surface reference points that are easily marked with colored ink. For more precise vascular mapping, we used correction processing to indicate blood vessels observed from a perspective perpendicular to the mapping sheet attached to the skin surface. Direct projection mapping to the body surface [16)] was initially considered; however, setting up a projection system in an operating room was deemed too complicated. We therefore decided to preoperatively prepare a mapping sheet using the projection method. The present findings indicate that this mapping sheet method was useful for denoting ALT perforator positions and courses. In addition, the mapping sheets had to be manually prepared in this clinical trial, but we expect this process to be automated in the future. We aim to provide more accurate and informative vascular maps with shorter time to expend.

Advantages of vascular mapping surgery based on PAT imaging include its non-invasiveness, high-resolution images, simplicity, automated operation, and low time requirement for operators. Our ultimate purpose is to improve the safety and applicability of thinning procedures and complex flap design. In order to conduct thinning surgery safely, it is important to preserve the linking vessels that connect perforators in the adipose layer. Furthermore, detailed information on the subcutaneous vessels enables surgeons to design complex flaps more easily without reducing the blood supply. Although US is another method for superficial vascular visualization, the detectable area is too limited to make comprehensive mapping sheets [17]. Furthermore, Doppler US has difficulty visualizing horizontally coursing vessels. CT angiography is useful for predicting the septocutaneous or intramuscular course of perforators; however, the visualization of subcutaneous branches *in vivo* is difficult without a high dose of contrast medium. We believe that PAT imaging-based perforator mapping surgery will become a breakthrough approach to overcoming these problems.

In terms of study limitations, skin incision and intraoperative retraction result in errors, which may be more significant if fat tissue is thicker. We hope that these errors will be decreased by additional technical refinements such as intraoperative direct projection mapping for the back-side of flaps and real-time intraoperative image processing. Also, we showed that the PAT-predicted stem portions of perforators matched the intraoperative surgical findings at the deep fascia level in a small number of cases.

We may be able to increase the number of cases by creating the mapping sheet more rapidly using automated tracing and printing systems. The next important research goal is to clarify the subcutaneous linking vessels directly to make the thinning procedure more reliable.

In addition to the limitations mentioned above, PAT has 2 technical drawbacks. First, arteries cannot be easily differentiated from veins. The morphological appearance of the triple-bundle pattern aids in the identification of perforators; however, it is desirable to visualize arteries and veins separately for perforator mapping. In 2018, our group successfully differentiated peripheral arteries from veins based on the difference in the oxygen saturation calculated from 2 wavelength measurements; this difference was called the S-factor [18]. Since the present study was started in 2017, it did not include the S-factor, but future trials will include the arterial visualization of perforators and linking vessels. Second, PAT imaging has what is known as the limited view problem [19], wherein it is difficult to visualize blood vessels in the vertical direction. While we expect further technical progress in the future, obtaining information on vessels in the horizontal and oblique directions is most important at present, as our ultimate purpose is vascular mapping for thinning procedures. We believe that this information about linking vessels will help support their preservation in thinned flaps and flaps with complex designs.

Conclusions

We developed a body-attachable vascular map based on PAT imaging for use in ALT flap surgeries. We found that PAT imaging was accurate in comparison with intraoperative surgical findings.

References

1) Koshima I, Fukuda H, Yamamoto H, Moriguchi T, Soeda S, Ohta S. Free anterolateral thigh flaps for reconstruction of head and neck defects. Plast Reconstr Surg 1993;92:421-428.

2) Schaverien M, Saint-Cyr M, Arbique G, Hatef D, Brown SA, Rohrich RJ. Three- and four-dimensional computed tomographic angiography and venography of the anterolateral thigh perforator flap. Plast Reconstr Surg 2008;121:1685-1696.

3) Alkureishi LW, Shaw-Dunn J, Ross GL. Effects of thinning the anterolateral thigh flap on the blood supply to the skin. Br J Plast Surg 2003;56:401-408.

4) Wang LV, Hu S. Photoacoustic tomography: in vivo imaging from organelles to organs. Science 2012;335:1458-1462.

5) Tsuge I, Saito S, Sekiguchi H, Yoshikawa A, Matsumoto Y, Toi M, Suzuki S. Photoacoustic tomography shows the branching pattern of anterolateral thigh perforators in vivo. Plast Reconstr Surg 2018;141:1288-1292.

6) Nagae K, Asao Y, Sudo Y, Murayama N, Tanaka Y, Ohira K, Ishida Y, Otsuka A,

Matsumoto Y, Saito S, Furu M, Murata K, Sekiguchi H, Kataoka M, Yoshikawa A, Ishii T, Togashi K, Shiina T, Kabashima K, Toi M, Yagi T. Real-time 3D photoacoustic visualization system with a wide field of view for imaging human limbs. F1000 Research 2018;7:1813.

7) Kitai T, Torii M, Sugie T, Kanao S, Mikami Y, Shiina T, Toi M. Photoacoustic mammography: initial clinical results. Breast Cancer 2014;21:146-153.

8) Fakhrejahani E, Torii M, Kitai T, Kanao S, Asao Y, Hashizume Y, Mikami Y, Yamaga I, Kataoka M, Sugie T, Takada M, Haga H, Togashi K, Shiina T, Toi M. Clinical report on the first prototype of a photoacoustic tomography system with dual illumination for breast cancer imaging. Plos One 2015:10;e0139113.

9) Toi M, Asao Y, Matsumoto Y, Sekiguchi H, Yoshikawa A, Takada M, Kataoka M, EndoT, Kawaguchi-Sakita N, Kawashima M, Fakhrejahani E, Kanao S, Yamaga I, Nakayama Y, Tokiwa M, Torii M, Yagi T, Sakurai T, Togashi K, Shiina T. Visualization of tumor related blood vessels in human breast by photoacoustic imaging system with a hemispherical detector array. Sci Rep 2017;7:41970.

10) American National Standards Institute. American national standard for safe use of lasers: American National Standards Institute, 2014. Available at: https://www.ansi.org/. Accessed June 10, 2015.

11) Sekiguchi H. Development of the rapid MIP viewer for PAT data – KURUMI: Kyoto University Rapid and Universal MIP Imager. IEICE Tech Report, Med Imaging 2017:116;163-167.

12) Imanishi N, Kishi K, Chang H, Nakajima H, Aiso S. Three-dimensional venous anatomy of the dermis observed using stereography. J Anat 2008;212:669-673.

13) Mun G, Kim H, Cha M, Kim W. Impact of perforator mapping using multidetector-row computed tomographic angiography on free thoracodorsal artery perforator flap transfer. Plast Reconstr Surg 2008;122:1079-1088.

14) Chae MP, Hunter-Smith D, Rozen WM. Comparative study of software techniques for 3D mapping of perforators in deep inferior epigastric artery perforator flap planning. Gland Surg 2016;5:99-106.

15) Shen Y, Huang J, Dong M, Li J, Ye W, Sun J. Application of computed tomography

angiography mapping and located template for accurate location of perforator in head and neck reconstruction with anterolateral thigh perforator flap. Plast Reconstr Surg 2016;137:1875-1885.

16) Hummelink S, Hameeteman M, Hoogeveen Y, Slump CH, Ulrich DJO, Kool LJS. Preliminary results using a newly developed projection method to visualize vascular anatomy prior to DIEP flap breast reconstruction. J Plast Reconstr Aesthet Surg 2015;68:390-394.

17) Debelmas A, Camuzard O, Aguilar P, Qassemyar Q. Reliability of color Doppler ultrasound imaging for the assessment of anterolateral thigh flap perforators: a prospective study of 30 perforators. Plast Reconstr Surg 2018;141:762-766.

18) Matsumoto Y, Asao Y, Sekiguchi H, Yoshikawa A, Ishii T, Nagae K, Kobayashi S, Tsuge I, Saito S, Takada M, Ishida Y, Kataoka M, Sakurai T, Yagi T, Kabashima K, Suzuki S, Togashi K, Shiina T, Toi M. Visualising peripheral arterioles and venules through high-resolution and large-area photoacoustic imaging. Sci Rep 2018;8:14930. doi:10.1038/s41598-018-33255-8.

19) Xu Y, Wang LV. Reconstructions in limited-view thermoacoustic tomography. Am Assoc Phys Med 2004;31:724-733.

Figure legends

Figure 1

(A) Reference markings of case 8 on the left thigh. The purple dots form a grid, with each dot separated by 4 cm. The red marks indicate the fascia-penetrating points of perforators detected by color Doppler US. (B) The anterolateral aspect of the left thigh is set in a tray of de-aired water with the patient in a semi-prone position.

Figure 2

An anteroposterior PAT image of case 8 in the all-layer view (A) and the deep-layer view (B). The color corresponds to the depth from the skin surface. The white arrow indicates the stem portion of the perforator estimated by PAT. Scale bar = 20 mm. (C) The a-b area shows an obliquely coursing branch from the stem portion of the perforator. The c-d area shows a horizontally coursing branch. (D) Microvessels connecting to the stem portion of the perforators are traced.

Figure 3

(A) Schematic illustration of the data correction for projection mapping. (B) Projection mapping is applied to the transparent film sheet after correction processing for 2-dimensional images. (C) The color indicates the depth, as follows: black ink = more than 9 mm, blue ink = 7-9 mm, red ink = less than 7 mm.

Figure 4

(A) The mapping sheets were attached to the thigh in case 3, in line with the dots marked before PAT imaging. The white arrows indicate the stem portions of the perforator estimated by PAT. The white arrowheads indicate the perforator detected by US at the deep fascia level. (B) Intraoperative findings of case 3. The black arrowheads indicate the three fascia-penetrating points of perforators that correspond to the results of PAT vascular mapping.

Supplemental figure 1

Intraoperative findings of case 3. (A) The area of thinning was planned based on the PAT mapping sheet. (B) The distal part of the ALT was thinned from 12 mm to 5 mm. (C) The portion marked by black arrowheads was used to cover the oropharyngeal upper wall.

Tables

Table 1. Schedule from PAT imaging to surgery

Day 1	PAT imaging	• US test with marking of reference points
		• PAT imaging
Day 2	Tracing	• Selection of perforator vessels
		• Tracing and correction for projection mapping
Day 3	Projection	• Projection mapping onto film sheets
		• Manual description with three color codes
Day 4	Sterilization	• Sterilization of vascular mapping sheets
Day 8*	Surgery	• Attachment of mapping sheets to the body surface
		• Incision with film sheets
		• ALT flap elevation
		*The day of surgery ranged from Days 8 to 11.

Table. 2 Results of PAT and Operative Findings

Patient	Age (years)	Sex	Height (cm)	Weight (kg)	Body Mass Index (kg/m^2)	Diagnosis	Side of ALT Flap	Size of ALT Flap (cm)	US Findings		PAT Findings		Operative Findings		
									Number of Perforators	Depth of Fascia (mm)	Number of Perforators	Types* of Perforators	Number of Perforators	Thinning Procedure (mm)	Complication
1	32	M	179	83	25.9	Chest wall sarcoma	Left	20 × 12	2	12	2	II+II	2	None	None
2	78	F	149	45	20.3	Buccal mucosal cancer	Right	33 × 10	2	8	3	II+II+III	3	None	None
3	53	F	158	44	17.6	Oropharyngeal cancer	Right	12 × 6	3	12	3	I+II+II	3	12→5	None
4	48	M	172	67	22.6	Buccal mucosal cancer	Right	25 × 7	1	12	1	II	1	None	None
5	67	M	174	71	23.5	Maxillary cancer	Right	28 × 8	2	10	2	III+III	2	None	None
6	49	M	168	65	23	Tongue cancer	Left	18 × 6	2	8	2	I+II	2	None	None
7	79	F	149	49	22.1	Pharyngeal fistula	Left	20 × 6	2	16	1	I	1	16→5	None
8	72	M	167	84	30.1	Nasal skin cancer	Left	27 × 8	2	10	2	II+III	2	None	None
Average	60		165	64	23.1		L/R=1	23 × 8	2	11	2		2		

*: classification of Shaverien M et al. [2)]

Figure 1

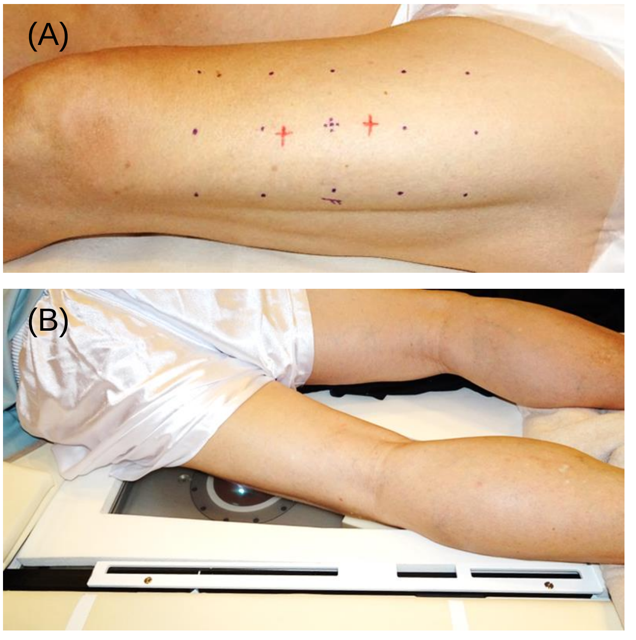

Figure 2

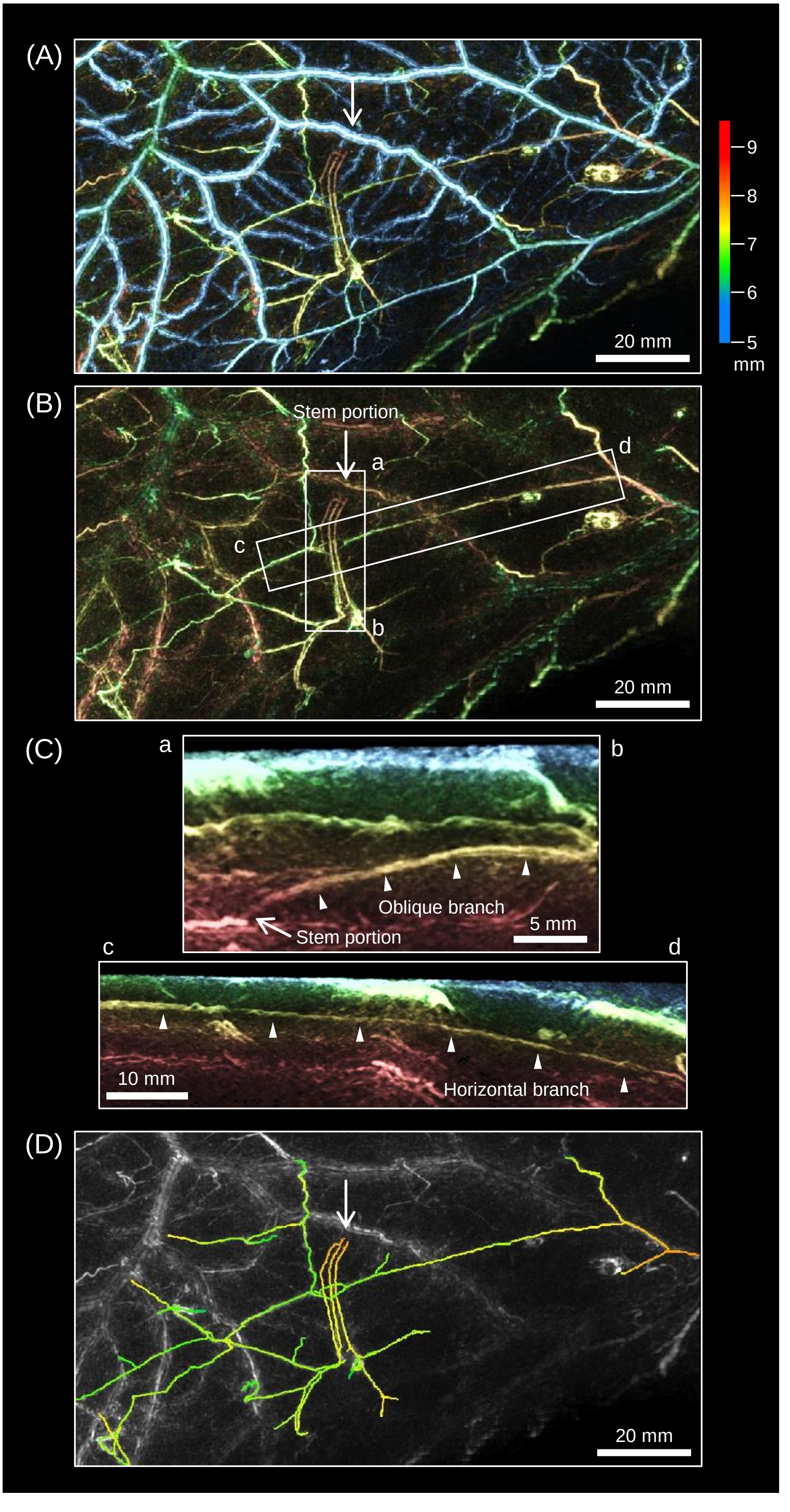

(A)
20 mm
9
8
7
6
5
mm
(B)
Stem portion
a
b
c
d
20 mm
(C)
a
b
Oblique branch
Stem portion
5 mm
c
d
10 mm
Horizontal branch
(D)
20 mm

Figure 3

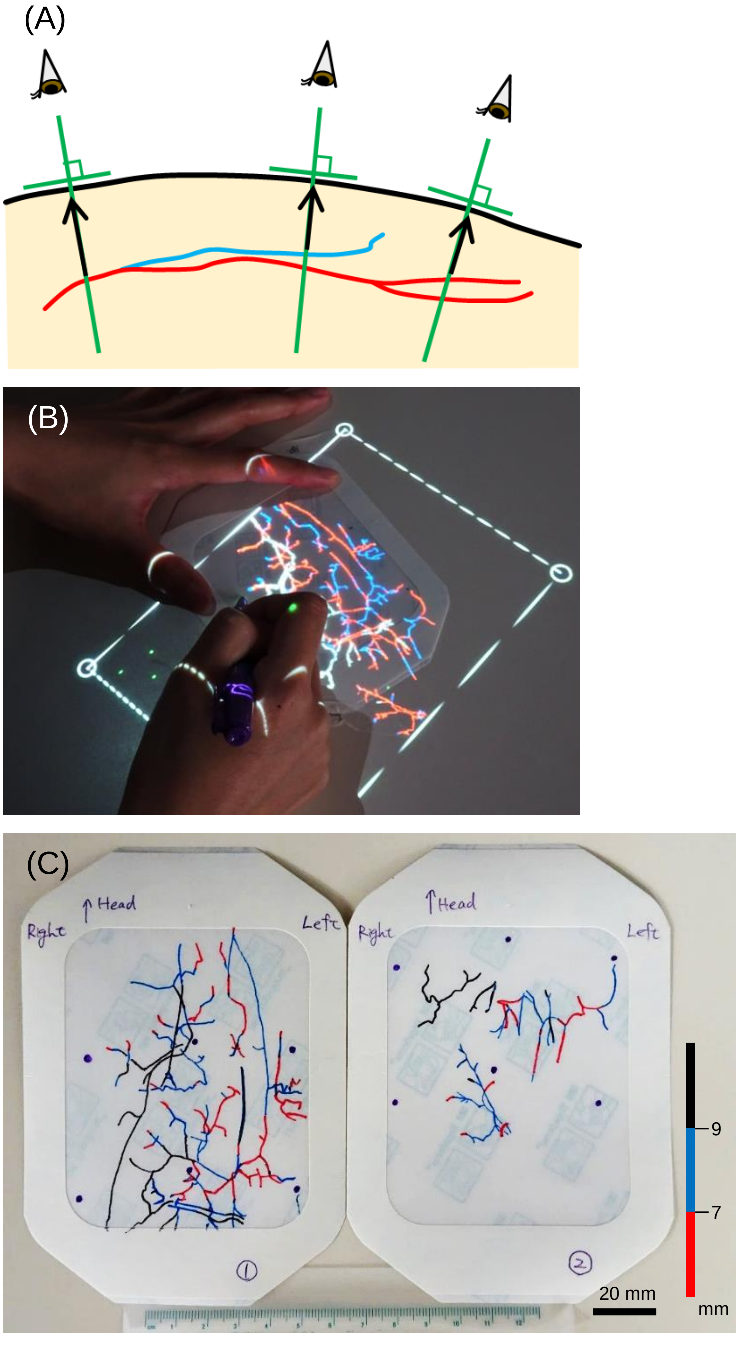

Figure 4

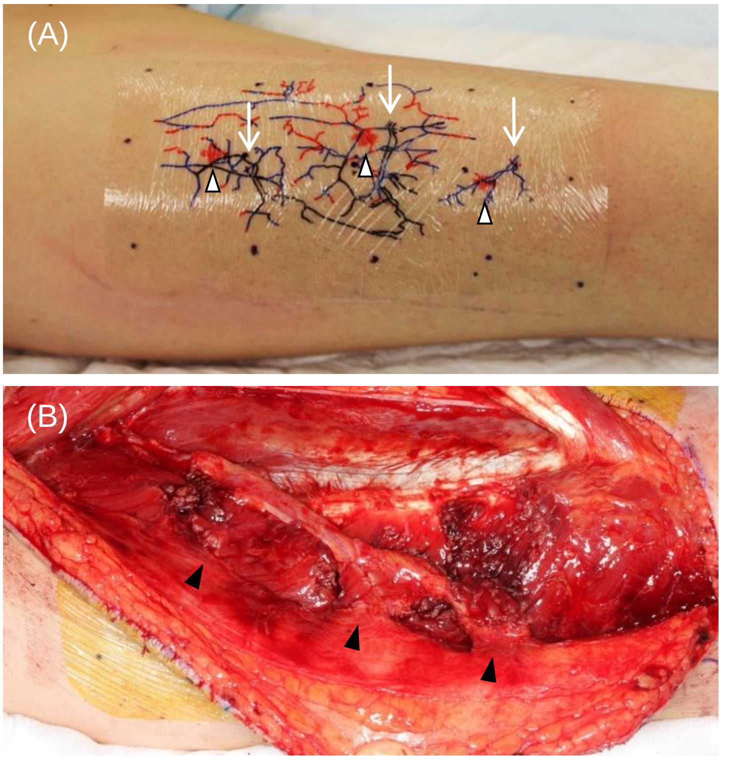

Supplemental 1